The International Journal of Advanced Manufacturing Technology (2023) 129:5679–5690
https://doi.org/10.1007/s00170-023-12668-4

ORIGINAL ARTICLE

Towards Salomon's hypothesis via ultra-high-speed cutting Ti-6Al-4V alloy

Ming-Yao Su[1,2] · De-Ru Wang[1,2] · Qi Wang[1,2] · Min-Qiang Jiang[1,2] · Lan-Hong Dai[1,2]

Received: 22 December 2022 / Accepted: 10 November 2023 / Published online: 22 November 2023

Abstract

Cutting temperature is a crucial factor in high-speed machining processes. In 1931, Dr. Carl Salomon proposed the fascinating hypothesis that the cutting temperature increases with the cutting speed to a critical point and then decreases as the cutting speed continues to climb, which provides a successive impetus for developing high-speed machining technology. Despite extensive studies over the past several decades, Salomon's hypothesis has not been fully verified. In this study, a unique measuring technique was developed, which combines a light gas gun-based ultra-high-speed cutting setup with an infrared detector-based high-speed transient temperature measuring system. Using this technique, the cutting temperatures for the most typically difficult-to-cut and widely used Ti-6Al-4V alloy are measured over a broad spectrum of cutting speeds ranging from 7.5 to 212.6 m/s. The experimental results show that the measured temperature at the tool tip first increases with increasing cutting speed to a critical point of 125.2 m/s and then decreases as the speed continues to increase, providing solid evidence for the Salomon's hypothesis. We further reveal that the tool temperature decreases at ultra-high cutting speeds stems mainly from less heat generation in the primary shear zone and more heat convection by high-speed chip flow.

Keywords Salomon's hypothesis · Cutting temperature · Ultra-high-speed cutting · Infrared detector

Nomenclature

a_c	Thermal diffusivity coefficient of the chip
c	Specific heat of material
h	Shear band width
Pe	Peclet number
t	Tool-chip contact time
t_0	Uncut chip thickness
T	Temperature
T_0	Ambient temperature
V	Cutting speed
V_c	Chip flow speed
V_s	Shear speed along the PSZ
W	Width of the primary shear zone
α	Tool rake angle
α_T	Thermal softening coefficient
$\dot{\gamma}$	Strain rate in the primary shear zone
λ_c	Thermal conductivity of the chip
ξ	Strain-rate hardening coefficient
ρ	Density of material
τ_0	The shear stress at the moment of shear instability
φ	Shear angle
χ	Evolution degree of shear band

✉ Lan-Hong Dai
lhdai@lnm.imech.ac.cn

[1] State Key Laboratory of Nonlinear Mechanics, Institute of Mechanics, Chinese Academy of Sciences, Beijing 100190, People's Republic of China

[2] School of Engineering Science, University of Chinese Academy of Sciences, Beijing 101408, People's Republic of China

1 Introduction

The cutting is one of the most widely used metal processing techniques for removing unwanted materials [1]. Extensive studies have been conducted on metal cutting because of its complex nature and economic importance. The development of metal cutting is generally aimed at improving processing efficiency by increasing the cutting speed. However, the high temperature generated in the cutting process significantly degrades tool life, machining precision, and power consumption [2]. In 1931, German engineer Dr. Carl Salomon proposed a fascinating hypothesis of high-speed cutting that the cutting temperature increases with increasing cutting speed up to a critical point and then decreases as the cutting speed continues to increase [3]. Nevertheless, this intriguing idea

is still under debate and has inspired many researchers to devote extensive efforts to identifying its existence [4–6].

Over the past 90 years, some studies have provided evidence to verify Salomon's hypothesis. Palmai [7] pointed out that Salomon's hypothesis is based on milling and can be explained by intermittent cutting. O'Sullivan and Cotterell [8] investigated the newly machined surface temperature using thermocouples and infrared thermography during aluminum turning experiments at cutting speeds ranging from 2.5 and 6.7 m/s. A decrease in the machined surface temperature was observed with the increase in cutting speed. Chen et al. [9] presented an inverse heat-transfer model combined with experiments to obtain the workpiece surface temperature in a high-speed milling aluminum process at cutting speeds ranging from 3.9 to 23.5 m/s. They found that a critical cutting speed exists, and the workpiece temperature decreases when the cutting speed is greater than the critical speed. Richardson et al. [10] also investigated the workpiece temperature in the dry milling of aluminum alloy with cutting speeds ranging from 5 to 79.1 m/s. They concluded that the heat conducted into the workpiece and workpiece temperature decreased as the cutting speed increased. Jiang et al. [11] carried out a series of experiments on slot milling of Ti-6Al-4V with cutting speeds ranging from 8.3 to 29.1 m/s. They reported that the tool temperature first increased and then decreased as the cutting speed increased.

On the orther hand, the validity of Salomon's hypothesis has also been questioned. Komanduri et al. [12] reviewed their research program and claimed that the chip-tool interface temperature increases with speed, approaching the melting point of the work material rather than falling off at very high speeds. Experimental measurements of the tool temperature during high-speed milling of Ti-6Al-4V were carried out by Li et al. [13]. Their results showed that the temperature increased with the cutting speed, and no reduction occurred at higher speeds. Abukhshim et al. [14] measured the temperature on the tool-chip contact face during high-speed turning of high-strength alloy steel at cutting speeds ranging between 3.3 and 20 m/s. They concluded that the rake face temperature increased gradually with the cutting speed. Sutter et al. [15] investigated the temperature fields during the high-speed cutting of low-carbon steel. They found that the maximal temperature in the chip increased continuously with an increase in speed from 10 to 65 m/s, and the temperature did not seem to tend towards the saturation point.

It is noted from the above review that the cutting temperatures has been defined in many different ways, referring to workpiece temperature, tool temperature, tool-chip contact face temperature, and chip temperature. There is still a lack of a well-defined cutting temperature that directly reflects the measurement results. Moreover, due to the spindle rotation speed limitation, the cutting speed in previous reports was relatively low and could not meet the critical point specified in the hypothesis. In addition, various measurement methods are used to measure the cutting temperature, including contact techniques (e.g., thermocouples [8, 10, 11, 13]) and non-contact techniques (e.g., thermal microscopy [9] and pyrometers [14, 15]). However, these techniques have the two main limitations: relatively low spatial resolution and long response time, which are unsuitable for the temperature measurement in ultra-high-speed cutting processes. Therefore, there is a strong need to develop advanced and reliable methods for achieving higher cutting speed beyond the critical point and measuring cutting temperature.

The main purpose of this study was to explore the validity of Salomon's hypothesis. To this end, the ultra-high-speed cutting device based on a light gas gun with an infrared detector-based high-speed transient temperature measuring system was developed to measure the tool temperature in ultra-high-speed cutting of the widely-used, but difficutlt-to-cut Ti-6Al-4V alloy. With this unique experimental device, the tool temperatures were precisely measured at cutting speeds ranging from 7.5 to 212.6 m/s. The evolution mechanism for the cutting temperature was discussed from the heat generation and convection during the ultra-high-speed cutting.

2 Materials and experimental setup

2.1 Workpiece material

The workpiece material used in the experiments was the titanium alloy Ti-6Al-4V, which is widely used in the industry because of its excellent mechanical properties and light density [16–18]. However, Ti-6Al-4V is a difficult-to-cut material because of its low thermal conductivity. Ti-6Al-4V is a typical cutting model material, and its speed threshold for high-speed cutting is relatively lower than that of other metallic materials such as copper, aluminum, and steel. The chemical composition of Ti-6Al-4V is shown in Table 1.

The optical microstructure of Ti-6Al-4V is shown in Fig. 1. The microstructures are composed of equiaxed α grains surrounded by a β phase. The workpieces are cutted into rectangles with dimensions of $40\times40\times2$ mm^3 by

Table 1 Chemical composition of Ti-6Al-4V

Elements	Al	V	Fe	C	N	H	O	Ti
wt (%)	5.99	4.2	0.2	0.01	0.004	0.005	0.1	Bal

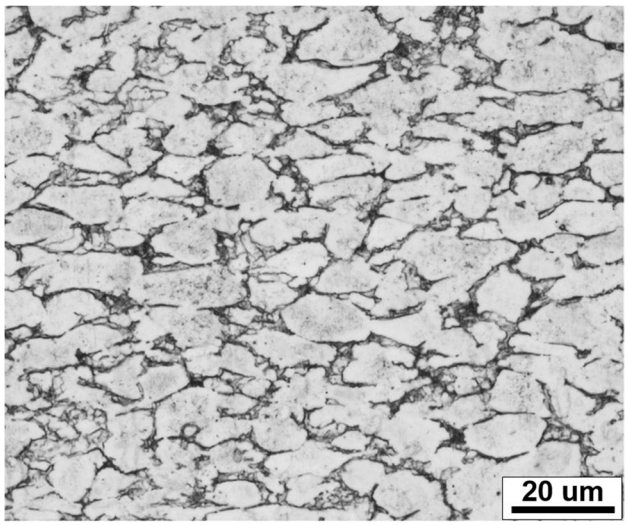

Fig. 1 The microstructures of Ti-6Al-4V after heat treatment

wire electrical discharge machining. Polishing was always necessary to obtain a close contact between the workpieces and tools.

2.2 Ultra-high-speed cutting setup

To achieve the ultra-high-speed cutting, a self-developed experimental device based on a light gas gun was set up [19] and is schematically presented in Fig. 2. The actual experimental setup is shown in Fig. 3. The workpiece holder is fixed on a Bakelite projectile, which is launched inside a tube by a 60 mm bore light gas gun. The workpiece moves with the Bakelite projectile guided in the launch tube to avoid rotation. A long launch tube (6 m) allows the projectile to reach a steady high speed. The velocities are measured using two laser emitter-receiver pairs placed on the end of the launch tube. The total weight of Bakelite projectile together with the workpiece and its holder is 0.7 kg, which can provide sufficient large kinetic energy to consume in the cutting process. Two symmetrical tool holders are aligned to cutting platform at the end of the launch tube. The tools are held in position inside the tool holders by means of setscrews. The cutting thickness can be precisely controlled by adjusting tool's position finely using a set of micrometer calipers. This design of fixed tools is convenient for measuring the temperature taken from the tool tip. Orthogonal cutting occurs when the workpiece impacts the tool. After the cutting is complete, the impact of projectile assembly is absorbed into a shock absorber. The cutting speed is controlled by adjusting the weight of the projectile and the pressure of the compressed gas in the gas gun.

In this way, we performed a series of cutting experiments over a wide range of speeds from 7.5 to 212.6 m/s. To the best of our knowledge, this is the highest cutting speed reported for the Ti-6Al-4V alloy. The cutting thickness (t_0) was set to be 200 μm. An uncoated tool of P10 tungsten carbide material was used in all the machining process. The tool was designed with the rake angle (α) 0° and clearance angle 5°. The width of the tools was 8 mm wider than that of the workpiece. This design ensures that the workpiece material can be successfully cut during each cutting process. In order to minimize the influence of the offset present between the workpiece and tool's side face (temperature measurement point) on the observed temperature, the upper surface of workpiece is set to align with the side of the cutting tool, which means that the offset is made as small as possible, and it can be approximately assumed that the temperature measured on the surface of the tool is the same as the actual temperature [20]. New cutting tools were used for each experiment to minimize the influence of tool wear on the experimental results.

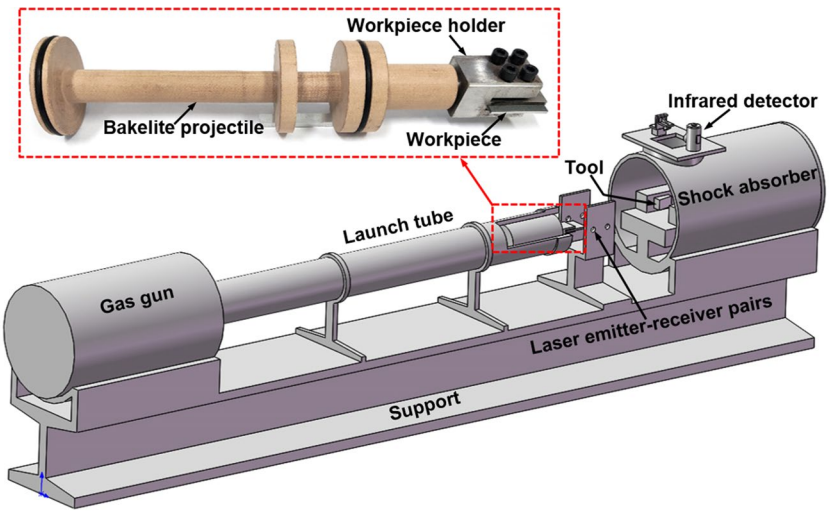

Fig. 2 Diagram of ultra-high-speed cutting setup based on a light gas gun. The insert shows the real projectile assembly

Fig. 3 The actual ultra-high-speed cutting experimental setup. The insert shows the cutting platform

2.3 High-speed transient temperature measuring system

Non-contact temperature measurement techniques are based on the fact that infrared radiation is continuously emitted from any body at the temperature above absolute zero and that the determination of this infrared radiation provides a sensitive temperature measurement. During cutting process, a considerable amount of heat is generated in the primary shear zone (PSZ) due to the high-strain-rate plastic deformation and in the secondary shear zone (SSZ) due to the friction between the chip and the tool. As a result, the tool is heated and emits infrared radiation from its surface. Here, this emitted infrared radiation is measured using a high-speed infrared dectector. The cutting temperature is obtained by a calibration experiment with respect to the measured infrared radiation expressed as an output voltage from the infrared dectector.

In this study, the high-speed transient temperature measuring system mainly included an infrared detector, optical system, and digital oscilloscope, as shown in Fig. 4. A single photoconductive mercury-cadmium-tellerium (HgCdTe) infrared detector was used in this temperature measuring system. This detector was highly sensitive to the radiation wavelength in the range 2–13 μm with a response time of approximately 1 μs. The element of the detector was a $100 \times 100\ \mu m^2$ square located behind a sapphire window in a liquid nitrogen dewar. This cooled the detector to 77K to minimize the thermal noise and maximize the sensitivity of the detectors. The signals passed through pre-amplifier

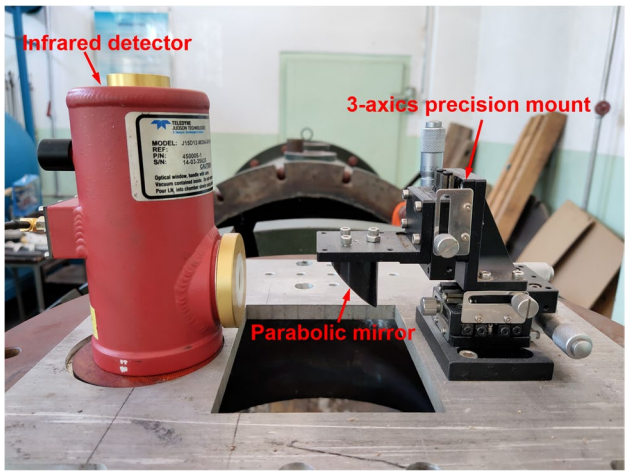

Fig. 4 The actual high-speed temperature measuring system

and were recorded on a digital oscilloscope. The frequency response of detector-amplifier combination was nominally between 10 Hz and 1 MHz. This lower limit frequency ensured that the system would not be significantly affected by low-frequency background radiation noise whereas the upper cutoff frequency corresponded to the detectable response time of about 1 μs. This system guaranteed a sufficient resolution to measure the transient temperature for very high cutting speed. It is important to note that the single infrared detector was performed over a small and finite area and thus it measured the average surface temperature over the focused area on the tool tip. It is expected that the small size of the element will reduce the averaging effect and allow to achieve an accurate measurement of the temperature of tool tip during the cutting process.

An ideal optical system for the high-speed transient temperature measuring system will gather 100% of the emitted infrared radiation from a specified region of the target tool without distortion. In practice, however, only a fraction of the infrared radiation can be gathered and some geometric aberration is inevitable. In this experimental study, a single parabolic mirror with a gold coating was chosen as the optical system. Such gold coating enhanced the reflectivity of infrared radiation. Meanwhile, the parabolic mirror can rotate the emitted radiation 90° in order to achieve proper orientation of the detector. The magnification of the optical system was approximately 1 so that the size of measurement area was equal to element size of the detector.

3 Experimental procedure

In order to measure the temperature of the tool tip accurately, careful optical alignment of the system was performed to ensure that the detectors were focused correctly

on the tool tip. The voltage signal measured from infrared detector requires calibration to obtain temperature. It is also necessary to carry out the accurate calibration of the detector. The methods used to achieve these requirements are discussed below.

3.1 Alignment and positioning

The positioning of optical system was performed using a He-Ne laser device and a spectroscope. The laser device provided a visible and concentrated laser to illuminate the tool and mark detector. The spectroscope can split a horizontal laser beam into two vertical upward and downward paths. During the positioning correction, the laser beam projected to the spectroscope, and the laser beam was divided into two beam paths by the spectroscope. Firstly, the downward beam path was used to locate the tip of the cutting tool. Then, the upward beam path was employed to determine the position of the infrared detector. The upward beam path was reflected by the parabolic mirror into a screen mounted on the front of the infrared detector. A bright spot from the visible laser was observed on the screen and brought into focus by making fine adjustments to the position of the screen. Finally, the screen was replaced by the infrared detector and the alignment was optimized by adjusting the position of the infrared detector to maximize the detector output signal. The diagram of alignment and positioning of the optical system is shown in Fig. 5.

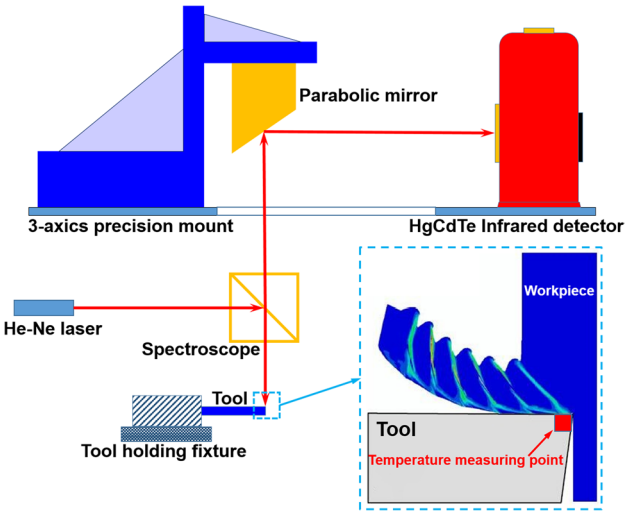

Fig. 5 The diagram of the alignment and positioning of the optical system

3.2 Calibration

Calibration of the infrared detector is crucial for reliable and accurate temperature measurement [21]. While it is possible to obtain a theoretical relationship between the detector output voltage and the tool temperature, it is difficult to accurately determine these parameters involved, such as the surface emissivity as a function of wavelength and temperature [22, 23]. Therefore, it is necessary to perform *in situ* experimental calibration that provides a direct relationship between the temperature on the surface of the tool and the output voltage of the infrared detector. This approach lumps all these parameters together and takes into account many unknown factors. Obviously, the conditions of the experimental calibration should be close to that of the actual experiment. The schematic diagram of the in situ experimental calibration is shown in Fig. 6.

A calibration sample was prepared for the same surface finish and kept at the same position as the actual test sample. A K-type thermocouple inserted into a small hole near the edge of the calibration sample. A minimal amount of thermal conductive paste was applied to the tips of the thermocouple to ensure good thermal contact between the

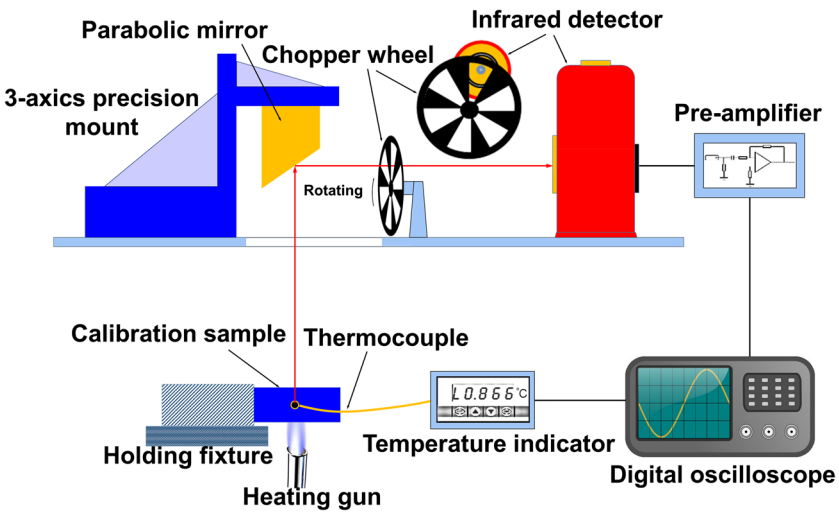

Fig. 6 The diagram of the in situ experimental calibration

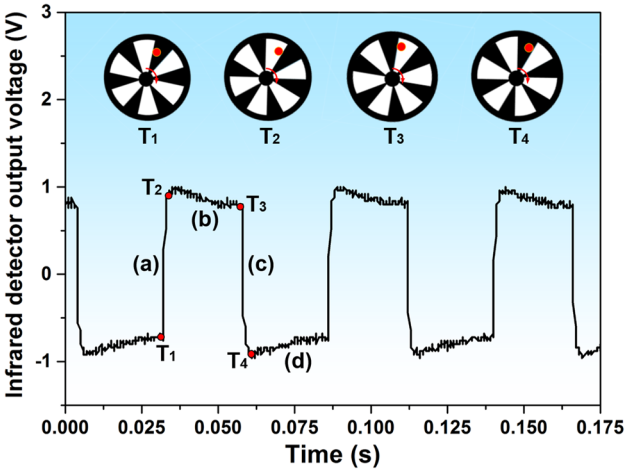

Fig. 7 A typical chopped output voltage signal from the calibration

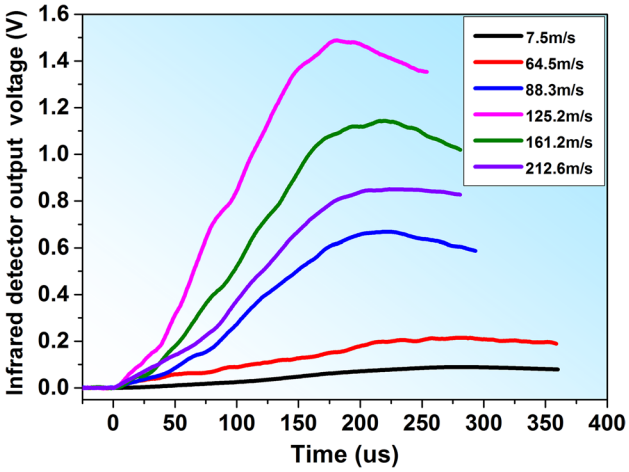

Fig. 9 The infrared detector output voltage signals of the ultra-high-speed cutting experiments under different cutting speeds

thermocouple and the calibration sample. The calibration sample was heated by a heating gun. During the heating process, a shield was placed between the specimen and the optical system. This is necessary to ensure that the optical system was not damaged by the direct heat from the heating gun. This is also required to make sure that the optical system itself was not heated, because this will bring an unwanted error signal to the detector. The calibration sample was heated to about 1200 °C and the heating gun was moved away from the experimental setup. As the sample cooled down, the shield was removed and the digital oscilloscope is triggered to start recording temperature data of thermocouple and output voltages of infrared detector simultaneously. Because the infrared detector was unable to measure constant or slowly changing radiation signal, a chopper was located between the optical system and the infrared detector to produce a pseudo AC signal. The calibration experiments were repeated multiple times to ensure repeatability of the results.

The signal of infrared detector during the calibration was recorded as the peak-to-peak voltage of the chopped signal. A typical chopped output voltage signal from the calibration is shown in Fig. 7, illustrating the different stages of data collection during the calibration. A nonlinear ramp was obtained because the chopped beam was circular. When the chopper passed through the center of the infrared beam, the rate of change of infrared radiation intensity entering the detector reached the maximum, corresponding to the maximum slope in regions (a) and (c). When the beam was either completely transmitted through the chopper or completely blocked by the chopper, infrared radiation intensity was approximately constant and the signal was effectively DC, corresponding to the top or bottom of the pulse in regions (b)

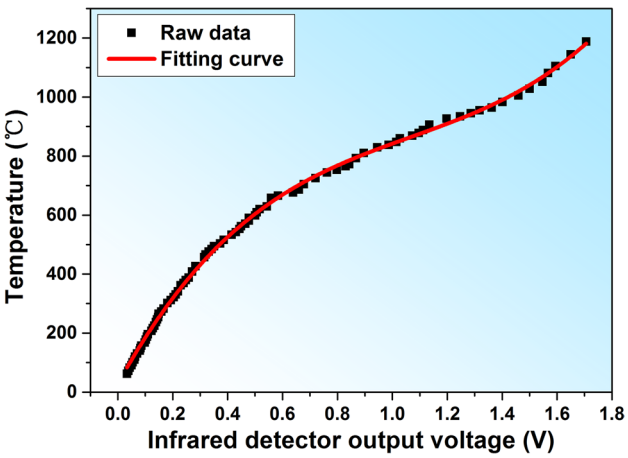

Fig. 8 The calibration curve of the infrared detector for the tool material

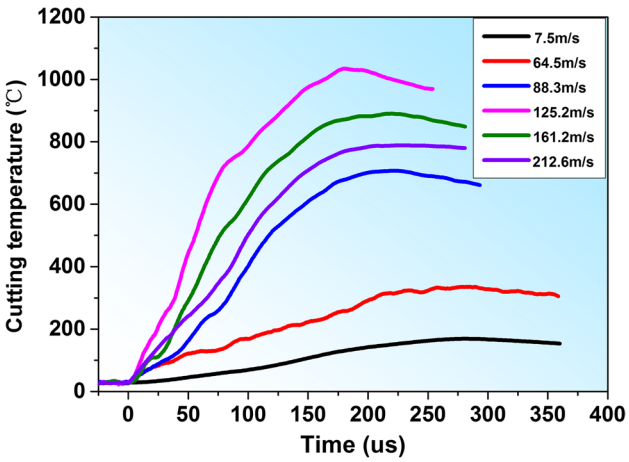

Fig. 10 The cutting temperature evolution of the tool tip under different cutting speeds

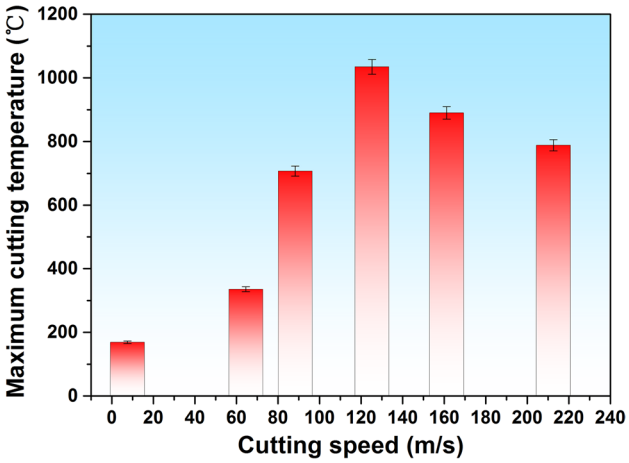

Fig. 11 The maximum cutting temperature located in the tool tip

and (d). Once the calibration was accomplished, the chopper was no longer required because continuous changes in temperature produce a transient response of the infrared detector during the actual ultra-high-speed cutting experiments.

The calibration experimental data of the infrared detector for the tool material is plotted in Fig. 8. In the present study, a third-order best-fitting curve of the calibration data was obtained. It should be noted that calibration experiments were carried out only for original tools and not for worn tool after the cutting experiment. Because the tools are sufficiently rigid compared to the workpiece, the tool did not show any significant deformation. Hence, the effects of change in surface condition (as a result of deformation) are negligible.

4 Results and discussion

4.1 Experimental results of the cutting temperature

A series of ultra-high-speed cutting experiments were conducted to obtain the tool temperature using an infrared detector versus cutting speeds. The dynamic characteristics of the cutting temperature in ultra-high-speed cutting of Ti-6Al-4V alloy were studied at various cutting speeds. Figure 9 shows the infrared detector output voltage signals

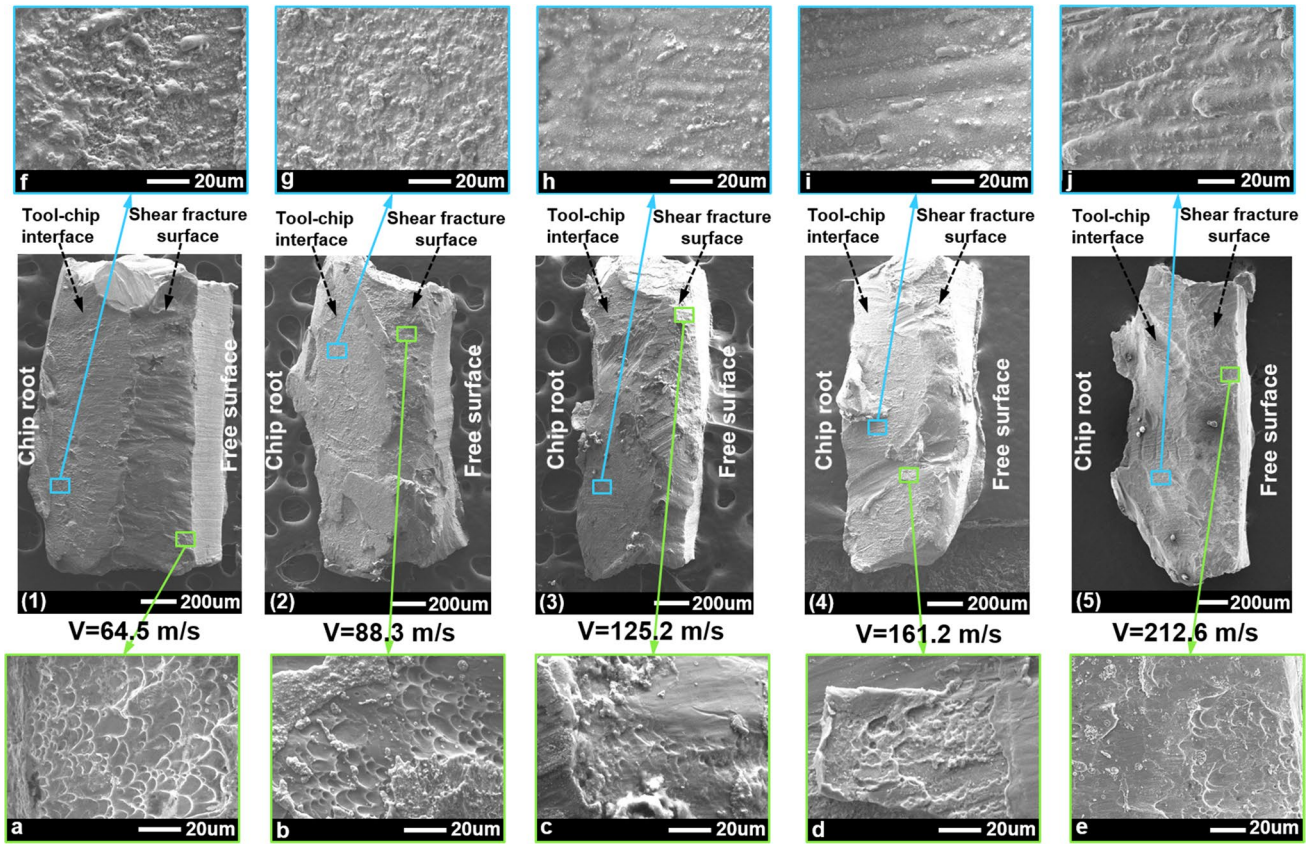

Fig. 12 Microstructures of shear fracture surface and the tool-chip interface at different cutting speeds. Shear fracture surface: a V = 64.5 m/s; b V = 88.3 m/s; c V = 125.2 m/s; d V = 161.2 m/s; e V = 212.6 m/s; tool-chip interface: f V = 64.5 m/s; g V = 88.3 m/s; h V = 125.2 m/s; i V = 161.2 m/s; j V = 212.6 m/s

Table 2 Thermo-mechanical properties and parameters of Ti-6Al-4V [32, 33]

Parameters	Value	Parameters	Value
ρ(kg m^{-3})	4430	$\dot{\gamma}_0$(s^{-1})	1.73×10^{-5}
a_c(m^2 s^{-1})	2.22×10^{-6}	τ_0(MPa)	2139.7
λ_c(W m^{-1} K^{-1})	6.6	T_0(K)	293
c(J kg^{-1} K^{-1})	670	α_T(K^{-1})	6.5×10^{-4}
φ(°)	45	ξ(Pa s^{-1})	0.75

of the ultra-high-speed cutting experiments under different cutting speeds 7.5, 64.5, 88.3, 125.2, 161.2, and 212.6 m/s. The infrared detector output voltage signals are converted into temperatures by utilizing the calibration curves shown in Fig. 10. The influence of the cutting speed on the maximum cutting temperature located in the tool tip is analyzed. Figure 11 shows that the measured maximum temperature at the tool tip first increases and then decreases with increasing cutting speed. The cutting temperature of the tool increased noticeably to a peak point of 1034 °C as the cutting speed increased to a critical speed of 125.2 m/s. When the cutting speed exceeded this critical speed, the temperature decreased as the cutting speed continued to increase. Interestingly, this experimental result is consistent with the Salomon's hypothesis [3].

We performed at least three independent experiments for each cutting speed to obtain averaged cutting temperature with reliable error bars, shown in Fig. 11. The sources of error in the cutting temperature measurements have numbers of components: the emissivity, the fluctuation, the calibration, and others issues. The emissivity is usually identified as the major error source [24]. The emissivity is related to change in the surface finish due to plastic deformation and oxidation. Since the strength and hardness of the tool material are far greater than those of the workpiece material, the tool can be considered as a rigid body without significant plastic deformation during the cutting process. Moreover, oxidation does not have enough time to form because the cutting happens in a very short time on the order of hundreds of microseconds. In our experiments, the tools do not show any obvious coloration after each experiment. Thus, the effect of the change in emissivity is negligible. The fluctuation is expected to be a large contributor to uncertainty in the cutting temperature. The fluctuations occur when the workpiece impacts the tool in high speed during the cutting process. These may be the slight movements in surface of the tool that cause some defocusing of the optical system. The contribution of this error is found to be approximately 2% [24]. The error in the calibration is from unwanted radiation that is not present during actual cutting experiments. While the calibration sample is heated during the calibration process, the atmosphere around the calibration sample and the apparatus near the sample may also become heated. This will add to the radiation transmitted into the infrared detector. In the case of actual experiments, the surrounding atmosphere and apparatus are not heated significantly. The error due to calibration is less than 0.2% [25].

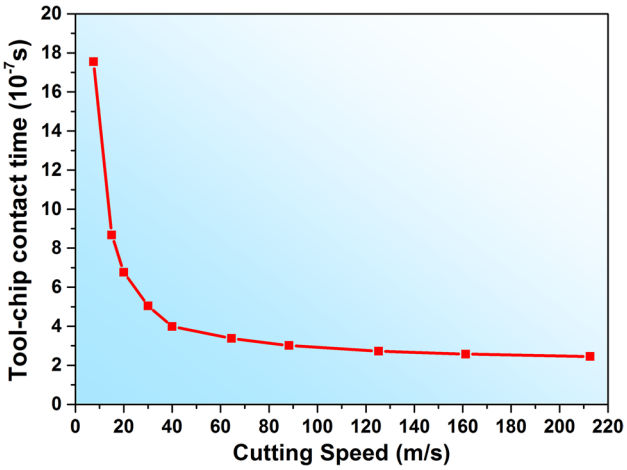

Fig. 13 The tool-chip contact time with different cutting speeds in the ultra-high-speed cutting

4.2 Effect of deformation state on cutting temperature

The transition of chip flow from continuously serrated to discontinuously fragmented was observed with increasing cutting speed to an ultra-high-speed level [26–28]. To explore the factors influencing the cutting temperature transition, chips at a cutting temperature near the maximum temperature were selected and evaluated using a scanning electron microscope (SEM). The microstructures of the shear fracture

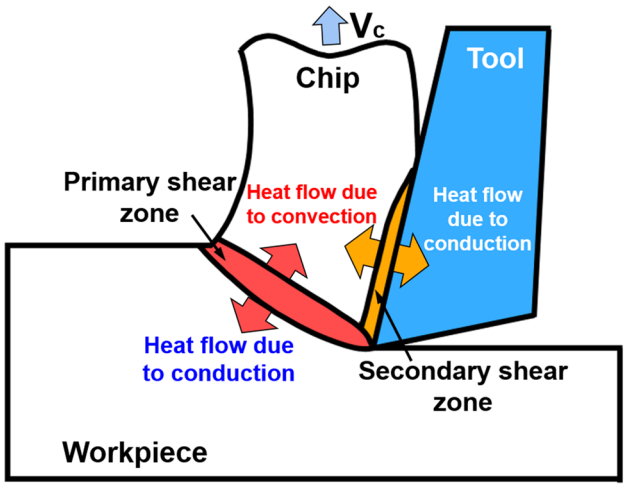

Fig. 14 Schematic diagram of heat generation zone and heat flows in the ultra-high-speed cutting

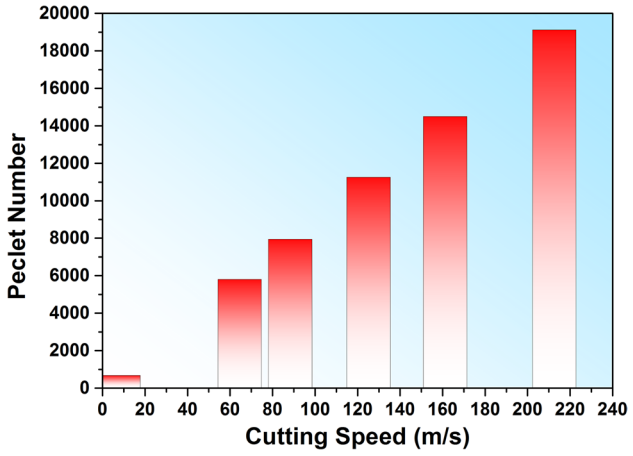

Fig. 15 Peclet number with different cutting speeds in the ultra-high-speed cutting

surfaces and the tool-chip interface of the segmented chips are shown in Fig. 12. At $V = 64.5$ m/s, elongated dimple structures are visible on the shear fracture surface (see Fig. 12a). This indicates that ductile shear fractures dominated the fragmented chip formation. Severe plastic deformation occurred, and a large amount of plastic work was converted into heat in the PSZ before chip fracture. Increasing the cutting speed to much higher values ($V = 88.3$, 125.2, 161.2, 212.6 m/s), the elongated dimples decrease while smooth areas increase (see Fig. 12b–e). This demonstrates the existence of a ductile-brittle transition during chip fracture [29, 30]. Therefore, the plastic shear deformation in the PSZ was restrained and the generated heat was reduced at a higher speed, leading to a decrease in the tool temperature.

Moreover, at $V = 64.5$ m/s, the molten droplets can be clearly observed on the tool-chip interface, as shown in Fig. 12f. The molten droplets are resulted from high temperature rise caused by the severe tool-chip friction. As the cutting speed increases to a higher level ($V = 88.3$, 125.2, 161.2, 212.6 m/s), the molten droplets gradually decreases until it disappears, but the flow traces of liquid chip materials become more visible on the tool-chip interface (see Fig. 12g–j). The tool-chip friction becomes more severe at higher cutting speed, and chip materials across the entire tool-chip surface melt [31]. Then, the flow traces of melted chip materials are left on the tool-chip interface after the chips separate from the rake face of tool. This indicates that the friction between the tool and chip in the SSZ was enchanced, and the generated heat was increased at a higher speed, leading to a tool temperature rise.

4.3 Effect of tool-chip contact time on cutting temperature

As mentioned in Section 4.2, the chips evolve from continuously serrated to fragmented when the cutting speed reaches an ultra-high-speed level. Fragmented chips are rapidly removed due to their high kinetic energy and separated from the tool. The fragmented chips resulted from a brittle fracture in the PSZ. Thus, the tool-chip contact time t was determined by the evolution time of the shear band deformation in the PSZ. Using the momentum diffusion-based shear band evolution model [32–34], the tool-chip contact time is derived as

$$t = \frac{1 - \alpha_T T_0}{\frac{\alpha_T \tau_0 V_s}{2\rho c h} - \frac{4\lambda_c}{3h^2} - \frac{2\lambda_c \xi V_s}{h^3 \tau_0}} \tag{1}$$

where V_s is the shear speed along the PSZ, $V_s = V cos\alpha / cos(\varphi - \alpha)$.

The width of PSZ (W) is set to be 1/10 of the uncut chip thickness, and the shear band width h is given by the following expression [32, 35]:

$$h = \chi \cdot W \tag{2}$$

The degree of shear band evolution χ used in Eq. (2) can be expressed as follows [32]:

$$\chi = 0.160 \times \left(\dot{\gamma}/10^6\right)^{0.65}, 0 < \dot{\gamma} \le 1.5 \times 10^6 \tag{3a}$$

$$\chi = 0.208 + 0.03 \times \left(\dot{\gamma}/10^6 - 1.5\right), \dot{\gamma} > 1.5 \times 10^6 \tag{3b}$$

where $\dot{\gamma}$ is the strain rate in the PSZ, $\dot{\gamma} = V\ cos\ \alpha / [h\ cos\ (\varphi - \alpha)]$.

The thermo-mechanical properties and parameters used to describe the behavior of Ti-6Al-4V are listed in Table 2 [32, 33]. The variation in the tool-chip contact time with the cutting speed is shown in Fig. 13. The tool-chip contact time decreased as the cutting speed increased. This indicates that there is less time for the heat generated by all the heat sources, especially the friction heat source transferred to the tool. As a result, the heat transferred along the tool-chip interface at high cutting speeds enters the tool much less, making the tool temperature lower than that at low cutting speeds.

4.4 Effect of material convection on cutting temperature

Heat generation occurred mainly in the PSZ and the SSZ during the cutting process [36]. In the PSZ, the heat due to shear plastic deformation may transfer to the chips by convection and to the workpiece by conduction [37]. Heat is generated in the SSZ owing to the friction between the chip and the tool rake face at the tool-chip interface, which flows to the chips due to convection and to the tool due to conduction [37]. The heat generation zone and the directions of heat flows in the ultra-high-speed cutting are shown in Fig. 14. Therefore, there are two competitive mechanisms of the heat transfer: conduction that diverts part of the heat from heat generation

zone into workpiece or tool and convection that brings part of this heat into chips due to its high-speed motion.

Material convection induced by high-speed chip flow rapidly removes material from the PSZ, which carries heat and momentum outwards from the PSZ [32]. The Peclet number, which is widely used in the thermal analysis of cutting systems subjected to moving heat sources [32, 38], was used to investigate the effect of material convection on the cutting temperature. In metal cutting, it is expressed as:

$$Pe = \frac{V_c \cdot t_0}{a_c} \tag{4}$$

where V_c is the chip flow speed, $V_c = Vsin\varphi / cos(\varphi - \alpha)$.

The Peclet number is a dimensionless similarity number that characterizes the ratio between material convection and thermal conduction. When cutting speed is increasing, *Pe* becames large and most of the heat generated in PSZ is transferred through convection into chips compared to a fraction of heat into the workpiece. Correspondingly, more heat is diverted from SSZ into chips due to convection than conduction into the tool which is fixed relative to the frictional heat source [38, 39]. Increasing the cutting speed and uncut chip thickness increases the Peclet number *Pe*, and *Pe* can be significant when the cutting speed is sufficiently high. Figure 15 shows the variation in the Peclet number at different cutting speeds during ultra-high-speed cutting. It is clear from Fig. 15 that the Peclet number increased with increasing cutting speed, correspondingly, more cutting heat is taken away by chip flow through material convection at a higher cutting speed. The tool was not sufficiently heated, and the temperature of the tool was restricted. Consequently, the tool temperature was lower at higher cutting speeds, consistent with the previous discussion.

5 Conclusion

In this study, a novel infrared detector-based high-speed transient temperature measuring system combined with a light gas-gun-based ultra-high-speed cutting device was developed. The cutting temperatures for cutting Ti-6Al-4V alloy were measured over a broad spectrum of cutting speeds ranging from 7.5 to 212.6 m/s. The measured temperature at the cutting tool tip first increased and then decreased with increasing cutting speed, consistent with the Salomon's hypothesis. The underlying mechanism of this temperature evolution was unveiled. The major conclusions drawn from this study are as follows.

1) The present ultra-high-speed cutting experiments show that the temperature at the tool tip first increases and then decreases with increasing cutting speed from 7.5 to 212.6 m/s. This study provides valuable experimental evidence for verifying the Salomon's hypothesis.
2) Based on the microstructures of the shear fracture surface of the fragmented chips, the plastic shear deformation in the PSZ was restrained, and the generated heat was reduced, which led to a decrease in the tool temperature. From the microstructures of the tool-chip interface of the fragmented chips, the tool-chip friction in the SSZ was enchanced, and the generated heat was increased at a higher speed, leading to a tool temperature rise.
3) The tool-chip contact time decreased as the cutting speed increased. There is not enough time for the heat generated by all heat sources to transfer into the tool.
4) With an increase in cutting speed, the material convection effect is enhanced. More heat was effectively carried away by the high-speed chip flow through material convection.
5) Combined with the heat generation, the tool-chip contact time decreases, and the material convection effect, variation trend of the tool temperature verify the Salomon's hypothesis.

Author contribution Ming-Yao Su: investigation, methodology, formal analysis, data curation, writing—original draft. De-Ru Wang: investigation, methodology, formal analysis. Qi Wang: investigation, methodology. Min-Qiang Jiang: formal analysis, writing—review and editing. Lan-Hong Dai: conceptualization, methodology, resources, supervision, writing—review and editing.

Funding This work is financially supported by the NSFC Basic Science Center Program for "Multiscale Problems in Nonlinear Mechanics" (No. 11988102), the NSFC (No. 11790292), the Strategic Priority Research Program (No. XDB22040302 and No. XDB22040303), and the Key Research Program of Frontier Sciences (Grant No. QYZDJSSW-JSC011).

Data availability All data generated or analyzed in this study are included in this paper.

Code availability Not applicable.

Declarations

Ethics approval Not applicable.

Consent to participate All authors consent to their participate in the research of this manuscript.

Consent for publication The manuscript is approved by all its authors for publication.

Competing interest The authors declare no competing interests.

References

1. Shaw MC (2005) Metal cutting principles. Oxford University Press, New York

2. Taylor FW (1907) On the art of cutting metals. The American Society of Mechanical Engineers, New York
3. Salomon CJ (1931) Process for machining metals of similar acting materials when being worked by cutting tools. German patent, Number 523594
4. Longbottom JM, Lanham JD (2006) A review of research related to Salomon's hypothesis on cutting speeds and temperatures. Int J Mach Tool Manuf 46:1740–1747. https://doi.org/10.1016/j.ijmachtools.2005.12.001
5. Longbottom JM, Lanham JD (2005) Cutting temperature measurement while machining – a review. Aircr Eng Aerosp Technol 77:122–130. https://doi.org/10.1108/00022660510585956
6. Wang B, Liu Z, Cai Y, Luo X, Ma H, Song Q, Xiong Z (2021) Advancements in material removal mechanism and surface integrity of high speed metal cutting: a review. Int J Mach Tool Manuf 166:103744. https://doi.org/10.1016/j.ijmachtools.2021.103744
7. Pálmai Z (1987) Cutting temperature in intermittent cutting. Int J Mach Tool Manuf 27:261–274. https://doi.org/10.1016/S0890-6955(87)80055-X
8. O'Sullivan D, Cotterell M (2002) Workpiece temperature measurement in machining. Proc Inst Mech Eng Part B J Eng Manuf 216:135–139. https://doi.org/10.1243/0954405021519645
9. Chen M, Sun F, Wang H, Yuan R, Qu Z, Zhang S (2003) Experimental research on the dynamic characteristics of the cutting temperature in the process of high-speed milling. J Mater Process Technol 138:468–471. https://doi.org/10.1016/s0924-0136(03)00120-1
10. Richardson DJ, Keavey MA, Dailami F (2006) Modelling of cutting induced workpiece temperatures for dry milling. Int J Mach Tool Manuf 46:1139–1145. https://doi.org/10.1016/j.ijmachtools.2005.08.008
11. Jiang F, Liu Z, Yang F, Zhong Z, Sun S (2018) Investigations on tool temperature with heat conduction and heat convection in high-speed slot milling of Ti6Al4V. Int J Adv Manuf Technol 96:1847–1858. https://doi.org/10.1007/s00170-018-1733-3
12. Komanduri R, Flom DG, Lee M (1985) Highlights of the DARPA Advanced Machining Research Program. J Eng Ind 107:325–335. https://doi.org/10.1115/1.3186005
13. Li L, Chang H, Wang M, Zuo DW, He L (2004) Temperature measurement in high speed milling Ti6Al4V. Key Eng Mater 259-260:804–808. https://doi.org/10.4028/www.scientific.net/KEM.259-260.804
14. Abukhshim NA, Mativenga PT, Sheikh MA (2005) Investigation of heat partition in high speed turning of high strength alloy steel. Int J Mach Tool Manuf 45:1687–1695. https://doi.org/10.1016/j.ijmachtools.2005.03.008
15. Sutter G, Ranc N (2007) Temperature fields in a chip during high-speed orthogonal cutting—an experimental investigation. Int J Mach Tool Manuf 47:1507–1517. https://doi.org/10.1016/j.ijmachtools.2006.11.012
16. Arrazola PJ, Garay A, Iriarte LM, Armendia M, Marya S, Le Maître F (2009) Machinability of titanium alloys (Ti6Al4V and Ti555.3). J Mater Process Technol 209:2223–2230. https://doi.org/10.1016/j.jmatprotec.2008.06.020
17. M'Saoubi R, Axinte D, Soo SL, Nobel C, Attia H, Kappmeyer G, Engin S, Sim W-M (2015) High performance cutting of advanced aerospace alloys and composite materials. CIRP Ann 64:557–580. https://doi.org/10.1016/j.cirp.2015.05.002
18. Ming W, Chen J, An Q, Chen M (2019) Dynamic mechanical properties and machinability characteristics of selective laser melted and forged Ti6Al4V. J Mater Process Technol 271:284–292. https://doi.org/10.1016/j.jmatprotec.2019.04.015
19. Ye GG, Xue SF, Ma W, Jiang MQ, Ling Z, Tong XH, Dai LH (2012) Cutting AISI 1045 steel at very high speeds. Int J Mach Tool Manuf 56:1–9. https://doi.org/10.1016/j.ijmachtools.2011.12.009
20. Soler D, Childs THC, Arrazola PJ (2015) A note on interpreting tool temperature measurements from thermography. Mach Sci Technol 19:174–181. https://doi.org/10.1080/10910344.2014.991027
21. Vernaza-Peña KM, Mason JJ, Li M (2002) Experimental study of the temperature field generated during orthogonal machining of an aluminum alloy. Exp Mech 42:221–229. https://doi.org/10.1007/BF02410886
22. Zehnder AT, Rosakis AJ (1991) On the temperature distribution at the vicinity of dynamically propagating cracks in 4340 steel. J Mech Phys Solids 39:385–415. https://doi.org/10.1016/0022-5096(91)90019-K
23. Hijazi A, Sachidanandan S, Singh R, Madhavan V (2011) A calibrated dual-wavelength infrared thermometry approach with non-greybody compensation for machining temperature measurements. Meas Sci Technol 22:025106. https://doi.org/10.1088/0957-0233/22/2/025106
24. Davies MA, Yoon H, Schmitz TL, Burns TJ, Kennedy MD (2003) Calibrated thermal microscopy of the tool–chip interface in machining. Mach Sci Technol 7:167–190. https://doi.org/10.1081/MST-120022776
25. Macdougall D (2000) Determination of the plastic work converted to heat using radiometry. Exp Mech 40:298–306. https://doi.org/10.1007/BF02327503
26. Sutter G, List G (2013) Very high speed cutting of Ti–6Al–4V titanium alloy – change in morphology and mechanism of chip formation. Int J Mach Tool Manuf 66:37–43. https://doi.org/10.1016/j.ijmachtools.2012.11.004
27. Ye GG, Xue SF, Ma W, Dai LH (2017) Onset and evolution of discontinuously segmented chip flow in ultra-high-speed cutting Ti-6Al-4V. Int J Adv Manuf Technol 88:1161–1174. https://doi.org/10.1007/s00170-016-8847-2
28. Liu H, Xu X, Zhang J, Liu Z, He Y, Zhao W, Liu Z (2022) The state of the art for numerical simulations of the effect of the microstructure and its evolution in the metal-cutting processes. Int J Mach Tool Manuf 177:103890. https://doi.org/10.1016/j.ijmachtools.2022.103890
29. Liu H, Zhang J, Xu X, Zhao W (2018) Experimental study on fracture mechanism transformation in chip segmentation of Ti-6Al-4V alloys during high-speed machining. J Mater Process Technol 257:132–140. https://doi.org/10.1016/j.jmatprotec.2018.02.040
30. Zhang T, Jiang F, Huang H, Lu J, Wu Y, Jiang Z, Xu X (2021) Towards understanding the brittle–ductile transition in the extreme manufacturing. Int J Extreme Manuf 3:022001. https://doi.org/10.1088/2631-7990/abdfd7
31. Liang X, Liu Z, Wang B, Wang C, Cheung CF (2022) Friction behaviors in the metal cutting process: state of the art and future perspectives. Int J Extreme Manuf 5:012002. https://doi.org/10.1088/2631-7990/ac9e27
32. Ye GG, Xue SF, Jiang MQ, Tong XH, Dai LH (2013) Modeling periodic adiabatic shear band evolution during high speed machining Ti-6Al-4V alloy. Int J Plasticity 40:39–55. https://doi.org/10.1016/j.ijplas.2012.07.001
33. Cai SL, Dai LH (2014) Suppression of repeated adiabatic shear banding by dynamic large strain extrusion machining. J Mech Phys Solids 73:84–102. https://doi.org/10.1016/j.jmps.2014.09.004
34. Meyers MA (1994) Dynamic Behavior of Materials. John Wiley & Sons, New York
35. Huang J, Kalaitzidou K, Sutherland JW, Aifantis EC (2007) Validation of a predictive model for adiabatic shear band formation in chips produced via orthogonal machining. J Mech Behav Mater 18:243–264. https://doi.org/10.1515/JMBM.2007.18.4.243

36. Abukhshim NA, Mativenga PT, Sheikh MA (2006) Heat generation and temperature prediction in metal cutting: A review and implications for high speed machining. Int J Mach Tool Manuf 46:782–800. https://doi.org/10.1016/j.ijmachtools.2005.07.024
37. Hao G, Liu Z (2020) The heat partition into cutting tool at tool-chip contact interface during cutting process: a review. Int J Adv Manuf Technol 108:393–411. https://doi.org/10.1007/s00170-020-05404-9
38. Astakhov VP (1999) Metal cutting mechanics. CRC Press, Boca Raton
39. Möhring H-C, Kushner V, Storchak M, Stehle T (2018) Temperature calculation in cutting zones. CIRP Ann 67:61–64. https://doi.org/10.1016/j.cirp.2018.03.009